Spectroscopic Study of 'CO' and its Isotopic mm/Submillimeter Lines from Dark Cloud Lynds 183

R. S. Thampi[1,*] & L. Pagani[2]

[1]*Physical Research Laboratory (PRL), Navrangpura, Ahmedabad 380 009, India.*
[2]*LERMA & UMR 8112 du CNRS, Observatoire de Paris 61, Av. de l'Observatoire,
75014 Paris, France.*
e-mail: satheesh_t@yahoo.com

Abstract. We have made spectral line analysis of CO and its isotopic lines from dark cloud Lynds 183 (L183). Our dataset incorporates $^{12}CO(1-0)$, $^{13}CO(1-0)$ and $^{13}CO(2-1)$ lines using NRAO-12 m and $^{12}CO(3-2)$, $^{13}CO(3-2)$ lines using CSO-10 m telescopes, respectively. Observations suggest steep north-south (direction with respect to the offset position (0, 0)) temperature gradient in the cloud. These are likely to be caused by non-uniform, Inter Stellar Radiation Field (ISRF) illumination due to the shadow of nearby L134 cloud complex. As the emission of radiation depends on local properties like density and kinetic temperature, the present study attempts to deduce the irradiation contrast (and the resulting temperature difference) using 1D Monte Carlo radiative transfer code RATRAN. The model results accord with the observed data and shows a temperature difference of ~ 7 K mainly within the cloud envelope. This results in a non-uniform intensity distribution of both CO and its species.

Key words. Radiative transfer—molecular spectral lines—temperature gradient.

1. Introduction

Dark clouds, such as L183 (L134N), reveal complex molecular emission distributions that suggest differences in chemical abundances and density. L183 is considered as an oxygen-rich cloud (Pagani *et al.* 2000). Optical extinction towards the centre of L183 is at least $A_v \sim 6$ (Laureijs *et al.* 1991) and may exceed $A_v = 10$. The cloud core (0.12–0.20 pc) is surrounded by an extended (0.4 pc) low extinction ($A_v < 1$) envelope. The spectrum of L183, suggests the presence of several molecular species including ^{12}CO and ^{13}CO (Caldwell 1979); H_2CO^+ (Guêlin *et al.* 1982); CS (Snell *et al.* 1982); $C^{18}O$, CS, $H^{13}CO^+$, SO, NH_3, C_3H_2 (Swade 1989a, 1989b); DCO^+, $H^{13}CO^+$ (Juvela *et al.* 2002); ND_2H (Roueff *et al.* 2000); HC_3N, N_2H^+ (Dickens *et al.* 2000); $^{16}O^{18}O$ (Pagani *et al.* 1993; Marèchal *et al.* 1997). Depletion effects of N_2H^+ and CO have been reported in many dark clouds (Pagani *et al.* 2005). These prevent CO from being an accurate mass tracer for cold dense cores. Spectral profiles of several molecules and the theory of star formation indicate that L183 is probably not a quiescent core

(Jian-Jun Zhou *et al.* 2001). Thus, in order to know whether there is any star formation activity within the cloud or not, it is important to investigate the physical and chemical properties of these dark clouds.

Millimeter/submillimeter-wave emission line techniques permit large scale mapping of the environments of star formation through the use of CO and its isotopes. Physical conditions such as temperature, density profile, abundance and depletion of such species can be deduced from the analysis of spectral lines with the aid of radiative transfer models. For this, the excited state of the molecule must be well understood. Asymmetrical ^{13}CO lines in the starless dark clouds TMC2 and L183 were modelled in terms of inward motions (Myers 1980). Non-Local Thermodynamic Equilibrium (NLTE) Monte-Carlo-1D code for N_2H^+ and N_2D^+ radiative transfer, has been applied to the detailed analysis of the main prestellar cores in L183 (Pagani *et al.* 2007).

In this paper, we present the results of new mm/submm observations and their 1D radiative transfer modelling with the code RATRAN (Hogerheijde & van der Tak 2000) with a view to refine our understanding of the temperature gradient within the envelope.

2. Observations and analysis

Spectral data contains 225 spectra for each of ^{12}CO(1—0), ^{13}CO(1—0) and ^{13}CO(2—1) lines and were recorded using the NRAO-12 m telescope at Kitt Peak (Arizona) during December 1999 to February 2000. Further using CSO-10 m telescope, 98 spectra of ^{13}CO(3—2) line and 961 spectra of ^{12}CO(3—2) line were taken during January–March 2000. Major telescopic parameters such as system temperature (T_{sys}), velocity resolution (D_v), integration time (T_{integ}), etc., are listed in Table 1.

Data analysis was carried out using *Continuum and Line Analysis Single dish Software (CLASS)*, developed by the Gildas group of Grenoble. Baseline subtraction for all the spectra was carried out. For the spectral information Gaussian fits were made and in general a single Gaussian fit, gave good fits for almost all the observations. The various offset positions of observations and the corresponding local standard of rest

Table 1. Parameters of the observations.

RA (1950)	DEC (1950)	Line name	Rest frequency (GHz)	$T_{sys.}$ (K)	$T_{integ.}$ (min)	$D_v * 10^{-2}$
NRAO-12 m-MACII*						
15:51:30.000	−02:43:30.00	^{12}CO(1—0)	115.271	300–400	2–27	6.34
15:51:30.001	−02:43:30.00	^{13}CO(1—0)	110.200	169–236	2–4.5	6.64
15:51:30.000	−02:43:30.00	^{13}CO(2—1)	220.398	35–70	2–34.5	6.59
CSO-10 m-50 MHz*						
15:51:30.001	−02:43:31.00	^{12}CO(3—2)	345.795	40–310	0.4–1.6	4.19
15:51:30.001	−02:43:31.00	^{13}CO(3—2)	330.588	400–1650	0.6–7.5	8.77

*Telescope names.

Table 2. Input model parameters.

Parameter	^{12}CO-(1—0), (3—2)	^{13}CO-(1—0), (2—1), (3—2)
T (K)	Core–7.5	Core–7.5
$n(\mathrm{H_2})\,\mathrm{cm^{-3}}$	$3*10^4$	$3*10^4$
r_{core} (pc)	0.08	0.08
r_{cloud} (pc)	0.2	0.2
$n(\mathrm{CO})_{\mathrm{core}}\,\mathrm{cm^{-3}}$	7.5	0.0625
$V_{-\mathrm{edge}}$ (km s^{-1})	0.24	0.24
Δv_{turb} (km s^{-1})	0.903^a	0.903^a

^{a}Microturbulant broadening added to the thermal broadening.
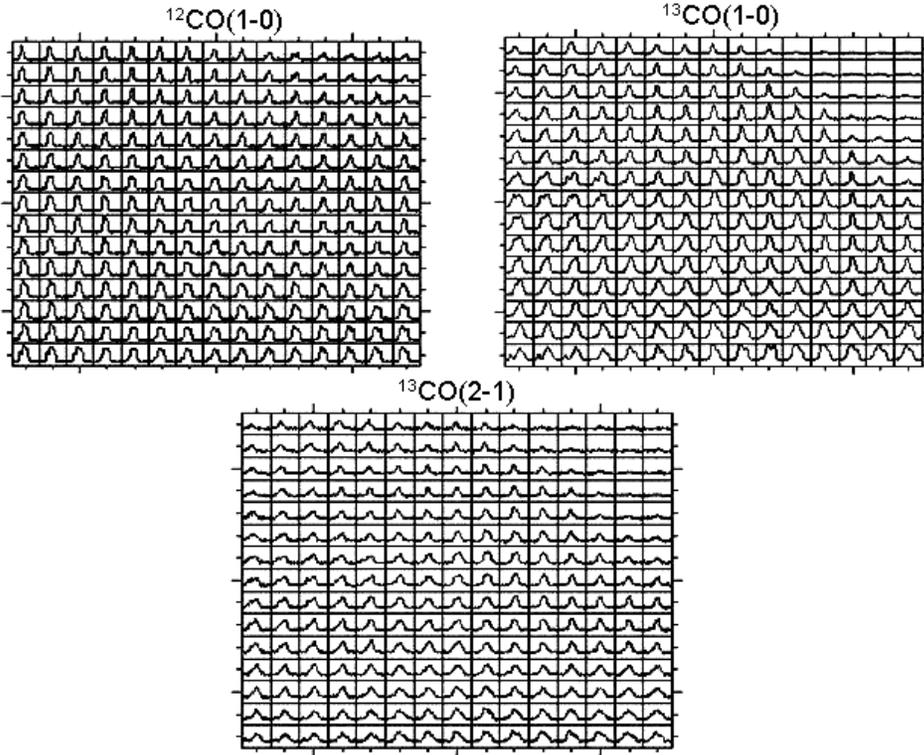
Figure 1. The three panels provide the spectral maps of ^{12}CO(1—0), ^{13}CO(1—0) and ^{13}CO(2—1). In the first panel, the velocity ranges from −2 to 8 km s^{-1} and the temperature ranges from −2 to 8 K. In the second and third panels corresponding velocities and temperatures ranges from −2 to 6 km s^{-1} and −2 to 5 K respectively. For each panel the offset positions of RA($\Delta\alpha$) and DEC($\Delta\delta$) are (7, 7), (−7, 7), (−7, −7) and (7, −7) (in arcmin) with respect to the center (0, 0) position (RA $= 15^{\mathrm{h}}51^{\mathrm{m}}30^{\mathrm{s}}$, DEC $= -2^0 43'31''$).

velocity (V_{LSR}) at the peak position, the intrinsic FWHM (as fitted by the CLASS) and, the integrated intensity ($\int T_A dv$) from observations as well as from the model are summarized in Table 3.
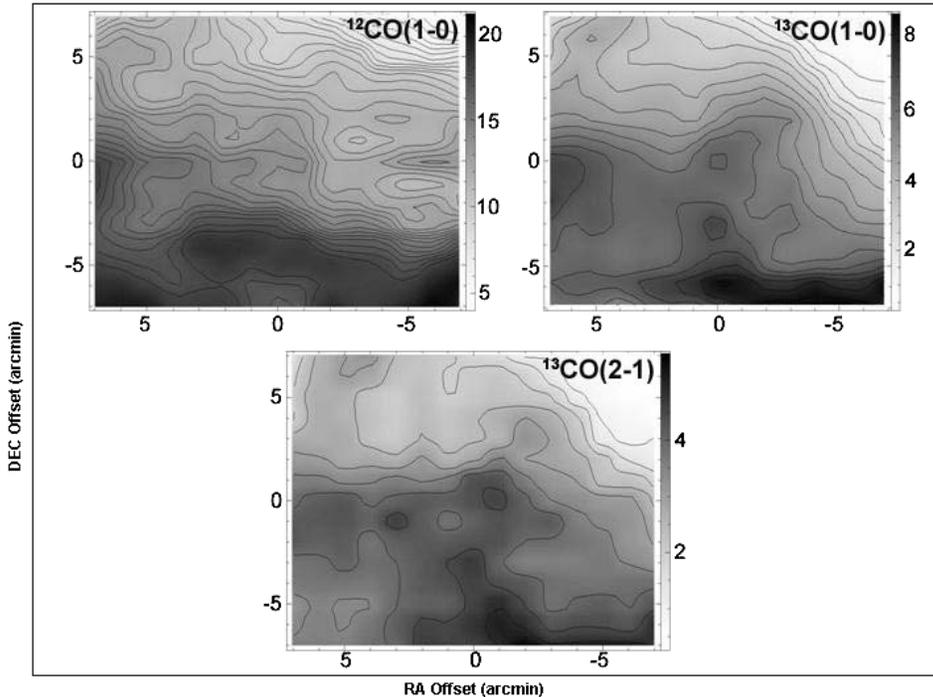
Figure 2. Integrated intensity contour maps for ^{12}CO(1—0), ^{13}CO(1—0) and ^{13}CO(2—1) transitions. The (0, 0) position is ($15^h51^m30^s$, $-2^043'31''$). Scales are in X-axis RA offset and Y-axis DEC offset (units are in arcmin, 1950).

3. Radiative transfer modelling

Using a 1-D Monte Carlo program for molecular radiative transfer (Hogerheijde & van der Tak 2000), we modelled all the observed spectral lines of ^{12}CO and ^{13}CO molecules. A cloud of size 0.4 pc was assumed for L183, for the modelling. Assuming a spherical symmetry, the model cloud consists of an inner dense core with uniform H_2 and CO densities. A core radius of 0.08 pc was assumed using the average for the characteristic size suggested by Swade (1989a, 1989b). We have used a cloud distance of 160 pc (Snell 1981) in our model. The core density was kept constant and a power law dependence ($n \sim r^{-2}$) was considered for the surrounding envelope. Initially a lower temperature of 8 K at the core and linearly increasing/decreasing temperatures up to a maximum of 12 K (Juvela *et al.* 2002) and minimum of 4.5 K at the envelope, were used. Best fits, however, were seen for a constant core temperature of 7.5 K and variable envelope temperature up to a maximum of 11.5 K. A constant dust temperature of 7.5 K (8 ± 0.5 K, Pagani *et al.* 2003) was used for the entire cloud regions. Though we have tried linearly increasing/decreasing dust temperature and constant dust temperature in our model, we found no significant change for the variable dust temperature and the most consistent and relatively better results we got for the constant dust temperature of 7.5 K. This could be probably due to the reason that cloud regions are dense enough and those optical and UV photons do not penetrate (absorbed in outer envelope). In general $T_{dust} < T_{gas}$ because gas is heated
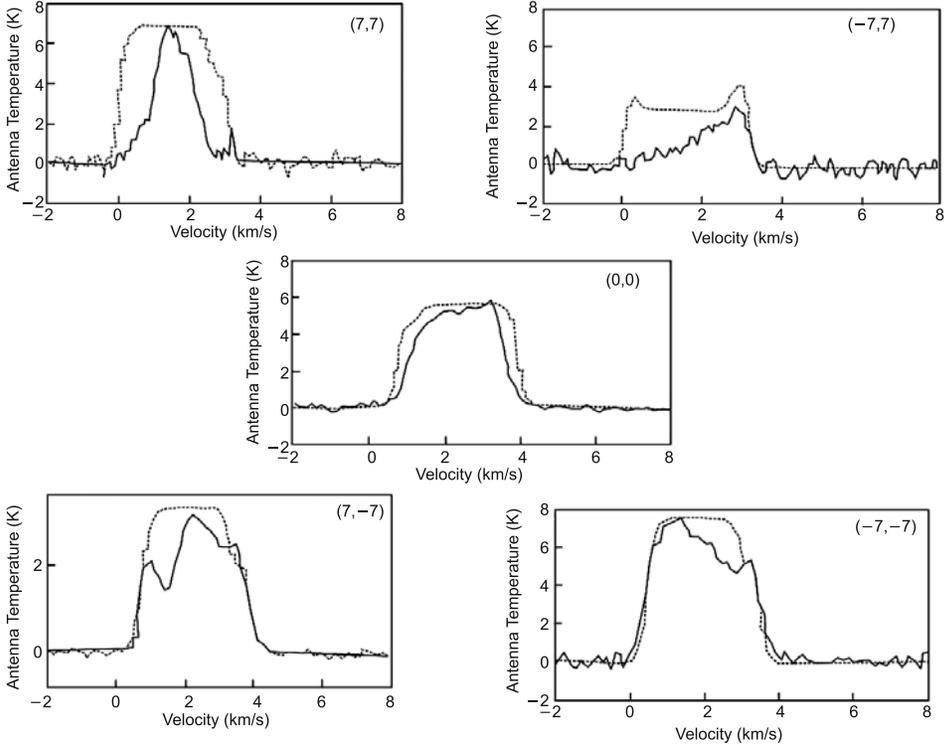
Figure 3. Comparison of modelled spectra (thick dotted line) with observed spectra (solid line) for $^{12}CO(1-0)$ line at few typical offset positions (mentioned within box) with respect to the $(0, 0)$ position (i.e., $15^h51^m30^s$, $-2^043'31''$). Scales are in X-axis velocity (km s^{-1}) and in Y-axis antenna temperature (K).

by cosmic rays at such high densities. Dust grains emit as black bodies and possibly due to this reason the temperature of dust is low as compared to that of the gas.

The 1D model calculations have Gaussian line shapes that were consistent with a thermal broadening with additional contribution from microturbulant broadening. A better fit is provided by models with velocities that increase linearly from the edge of the cloud to some maximum velocity at the edge of the core. Finally for the entire cloud we have the temperature, abundance, microturbulant line width and infall velocity ($v \sim r^{-0.5}$).

The cloud is illuminated by the Cosmic Microwave Background Radiation (CMBR) at a temperature of 2.7 K. Energy levels, statistical weights, radiative decay rates and collisional rate coefficients were taken from the default files of both ^{12}CO and ^{13}CO from the LAMDA database (Schöier *et al.* 2005). Parameters used for calculation are listed in Table 2. The best fit model that matches both ^{12}CO and ^{13}CO profiles has higher ^{12}CO density in the inner region and an outer, infalling envelope with a lower density. Variation in the turbulent broadening width also has a large effect on the line shape. A turbulent width of 0.2 km s^{-1} is necessary for the spectrum to be double peaked. In the present case the observed data, gave a best fit for a turbulent width of 0.9 km s^{-1} along with a thermal line width of 0.07 km s^{-1}.

Table 3. Comparison of observational results with the model.

Line	Offset $\Delta\alpha, \Delta\delta$ (arcmin)	Position (km s^{-1}) Obs.	FWHM (km s^{-1}) Obs.	$\int T_A dv$ (K · km s^{-1}) Obs.	Mod.	Kinetic temp. (K) (model) Core	Envelope
^{12}CO(1—0)	(7, −7)	2.39	2.49	7.7	7.9	7.5	11.5
	(−7, −7)	1.82	2.62	7.4	7.3	7.5	11
	(7, 7)	1.54	1.28	6.7	7.0	7.5	10.5
	(0, 0)	2.42	2.24	6.1	5.5	7.5	9
	(−7, 7)	2.50	1.50	2.5	3.3	7.5	6
^{12}CO(3—2)	(7.5, 7.5)	1.73	0.81	2.1	2.4	7.5	9
	(−7.5, 0)	2.48	1.52	2.3	2.3	7.5	8.5
	(7.5, 0)	2.21	1.83	2.7	2.3	7.5	8.5
	(0, 0)	3.04	1.73	2.3	4.1	7.5	11.5
^{13}CO(1—0)	(7, −7)	2.64	1.39	3.6	3.2	7.5	5.5
	(−7, −7)	2.32	1.73	4.3	4.4	7.5	8.5
	(7, 7)	1.71	0.94	2.1	2.1	7.5	4.5
	(0, 0)	2.67	1.23	5.0	5.0	7.5	9.5
^{13}CO(2—1)	(7, −7)	2.55	1.75	2.2	2.2	7.5	5
	(−7, −7)	2.28	2.11	2.7	2.6	7.5	6
	(7, 7)	1.67	1.24	1.1	1.0	7.5	4.5
	(0, 0)	2.68	1.38	3.2	3.0	7.5	8
^{13}CO(3—2)	(0, 0)	2.65	1.31	1.2	2.3	7.5	11.5
	(4, −4)	2.69	0.78	1.2	1.7	7.5	8.5
	(−0.5, −0.5)	2.72	1.39	1.3	2.3	7.5	11.5
	(0, 3.5)	2.51	0.61	1.3	1.6	7.5	7

Inputs to the radiative transfer model such as density, dust temperature, and velocity structure of the core and abundances of each molecule were taken from the standard references and used in case of L183 and are given in Table 2. However, many parameters are constrained by related observations and results. The remaining free parameters were then varied so as to fit the profiles of each of the two CO transitions. We have used the ratio of ^{12}C/^{13}C ~ 60 from the local interstellar medium value used by Miwa Goto *et al.* (2003).

4. Results and discussion

The analyzed spectra of CO and its isotopic lines show a line shape close to Gaussian. Reasonably good fits in both height and width were obtained for almost all observations of both molecules. Both the ^{12}CO and ^{13}CO transitions have signs of self-absorption indicating that some ^{12}CO and ^{13}CO molecules exist in a lower excited state in a foreground gas. Spectral maps of ^{12}CO(1—0), ^{13}CO(1—0) and ^{13}CO(2—1) cover practically the entire cloud and are shown in Fig. 1 and the corresponding integrated intensity contour maps are shown in Fig. 2. This map clearly reveals the non-uniform intensity distribution throughout the entire cloud region. Lines are more intense and broader in southern region of the cloud compared to that of the northern region.
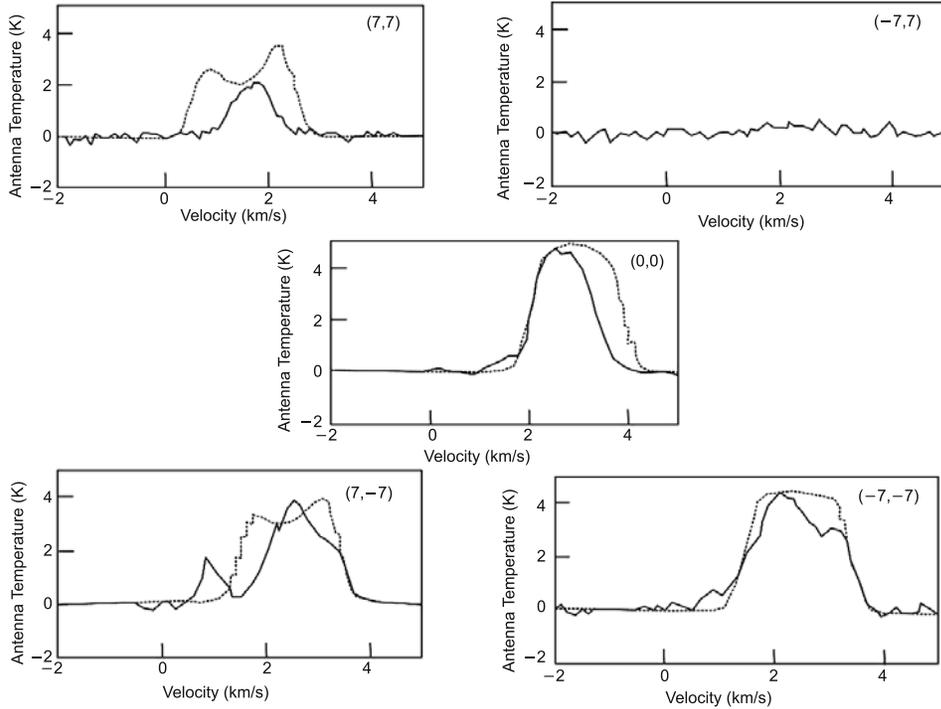
Figure 4. Comparison of modelled spectra (thick dotted line) with observed spectra (solid line) for $^{13}CO(1\!-\!0)$ line at few typical offset positions (mentioned within box) with respect to the (0, 0) position (i.e., $15^h51^m30^s$, $-2^043'31''$). Scales are in X-axis velocity (km s^{-1}) and in Y-axis antenna temperature (K).

The ^{12}CO lines seem to be more complex and diverse. They are much broader, more nearly 'flat-topped' due to self-absorption, the observations show slight asymmetry with respect to rest frequency. The ^{12}CO lines are saturated, and as a consequence only the outskirts of the cloud are visible. Here, the illumination seems to come from the bottom (there is a larger cloud below, L134, which might shield the northern part a bit from the interstellar radiation field, provoking this gradient).

The line width of all ^{12}CO and ^{13}CO lines varies marginally throughout the cloud. The average line width (FWHM) of $^{12}CO(1\!-\!0)$ line is 2 km s^{-1} and the average integrated intensity is 5.5 K·km s^{-1}. In the case $^{12}CO(3\!-\!2)$, the line width is 1.4 km s^{-1} and the average integrated intensity is 2.4 K·km s^{-1}. Similarly the $^{13}CO(1\!-\!0)$, $(2\!-\!1)$ and $(3\!-\!2)$ spectral lines look narrow at the centre and broader at the wings with a line width of 1.3, 1.6 and 0.6 km s^{-1}, respectively, and with an average integrated intensity of 3.5, 2.7 and 2.5 K·k ms^{-1} each. The intensity ratios of $^{12}CO/^{13}CO$ at various offset positions such as (0, 0), (7, -7) and (7, 7) are 1.2, 2.1 and 3.2 respectively, indicating the non-uniform distribution of both molecular species with respect to the temperature. Both $^{13}CO(1\!-\!0)$ line and $^{13}CO(3\!-\!2)$ have similar asymmetrical shapes with blue shifted peaks as that of lines (Myers 1980), suggestive of possible contraction of core along the observed lines of sight.
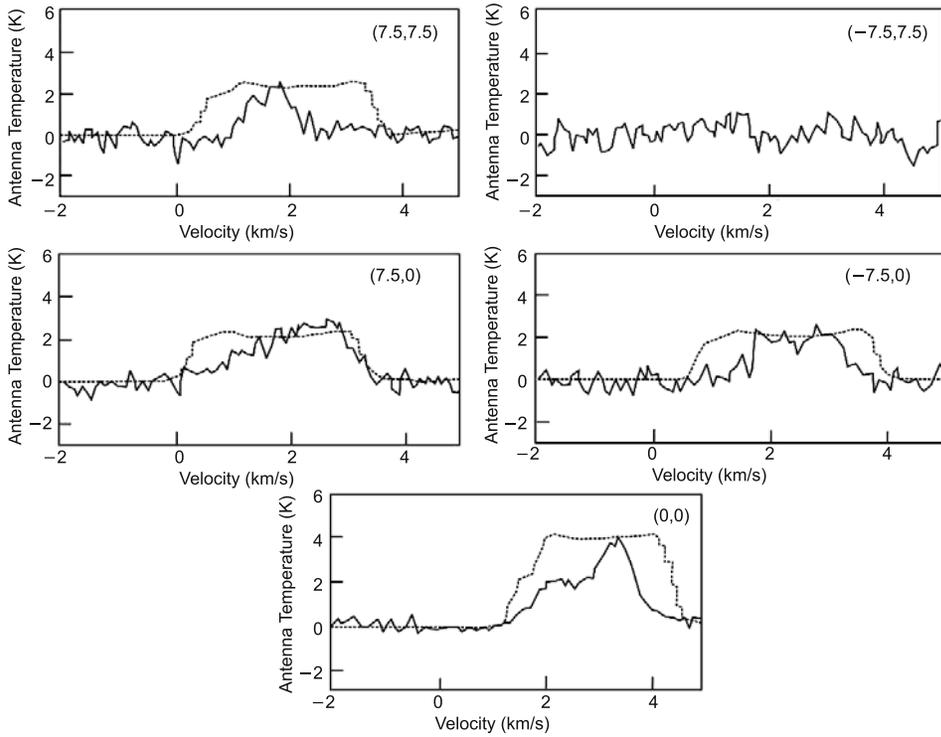
Figure 5. Comparison of modelled spectra (thick dotted line) with observed spectra (solid line) for ^{12}CO(3—2) line at few typical offset positions (mentioned within box) with respect to the (0, 0) position (i.e., $15^h51^m30^s$, $-2^043'31''$). Scales are in X-axis velocity (km s^{-1}) and in Y-axis antenna temperature (K).

The 1D model spectra of both CO species are compared with the observed ones and few typical comparisons for each species are shown in Figs. 3–7. The observed and the modelled spectra show similar trends in the wings and in the core. Observations of both CO species show reasonably good matching with the models especially in the southern part of the cloud. Intensity mismatch are more prominent in case of the observations taken towards the northern part of the cloud. We have tried to match these observations by changing the number density of both ^{12}CO and ^{13}CO and kinetic temperature up to 3 K, which fails probably because the lines are optically thick. An alternative reason could be the possible abundance variation of CO species because of freeze-out onto grains in the cold interiors of molecular cores (Brown *et al.* 1988; Willacy & Williams 1993).

We have compared our results with the observations (Vedi *et al.* 1985) of ^{12}CO $J = 3$—2 and new $J = 1$—0 transitions for the dark cloud L183. Vedi *et al.* predicted the radiation temperature for the two transitions as $T_R(3$—$2) = 4.1$ K and $T_R(1$—$0) = 7.5$ K, respectively. Among the two fundamentally different models that they have used, the first model, where L183 is considered to be a single large cloud, with the line of sight closer to the edge than the centre, and where a radially increasing temperature is attributed to UV heating by the interstellar medium, is almost similar to
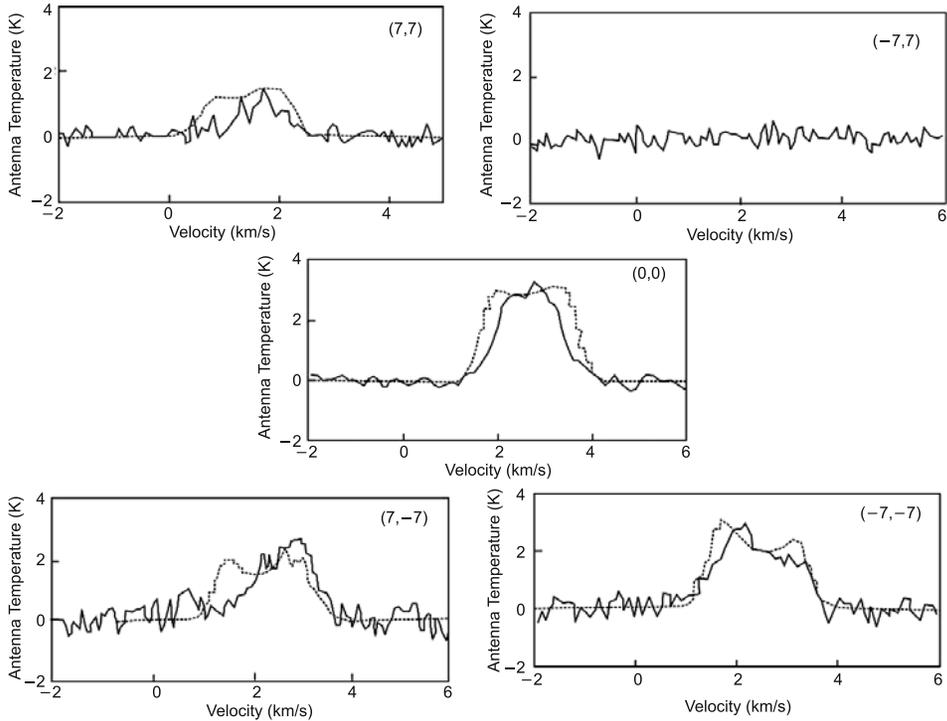
Figure 6. Comparison of modelled spectra (thick dotted line) with observed spectra (solid line) for ^{13}CO(2—1) line at few typical offset positions (mentioned within box) with respect to the (0, 0) position (i.e., $15^h51^m30^s$, $-2^0 43' 31''$). Scales are in X-axis velocity (km s^{-1}) and in Y-axis antenna temperature (K).

our parameterized modelling. Our model result shows (Table 3) a maximum kinetic temperature of 11.5 K in the southern part (offset position $(7, -7)$) of the cloud and a minimum of 6 K in the northern part $(-7, 7)$ of the cloud for a typical ^{12}CO(1—0) transition. In case of ^{12}CO(3—2) transition, a maximum kinetic temperature of 11.5 K at the central part $(0, 0)$ of the cloud and a minimum of 9 K in the northern part $(7.5, 7.5)$ of the cloud are observed. Similarly from the other observed CO transitions and corresponding models, we could observe a kinetic temperature difference of ~ 7 K throughout the envelope of the cloud. Our observed and modelled radiation temperature (7.5 K) agrees well with the predicted radiation temperature values for ^{12}CO(1—0) lines, as reported (7.5 K in Vedi *et al.* 1985) in some (mostly southern) part of the cloud. A typical example at offset position $(-7, -7)$ is shown in Fig. 3 for the ^{12}CO(1—0) transition. From the figure it is clear that the radiation temperature values change significantly in the northern part $(-7, 7)$ of the cloud from the predicted value suggesting a steep north to south temperature gradient within the cloud envelope. In case of ^{12}CO(3—2), we could find the radiation temperature almost matches with their predicted value of ~ 4.1 K (Vedi *et al.* 1985) at the central part $(0, 0)$ and shows (in Fig. 5) the temperature gradient from the north to the central part of the cloud. Similar trend is observed for all other transitions, which confirms a clear-cut steep temperature gradient throughout the envelope.
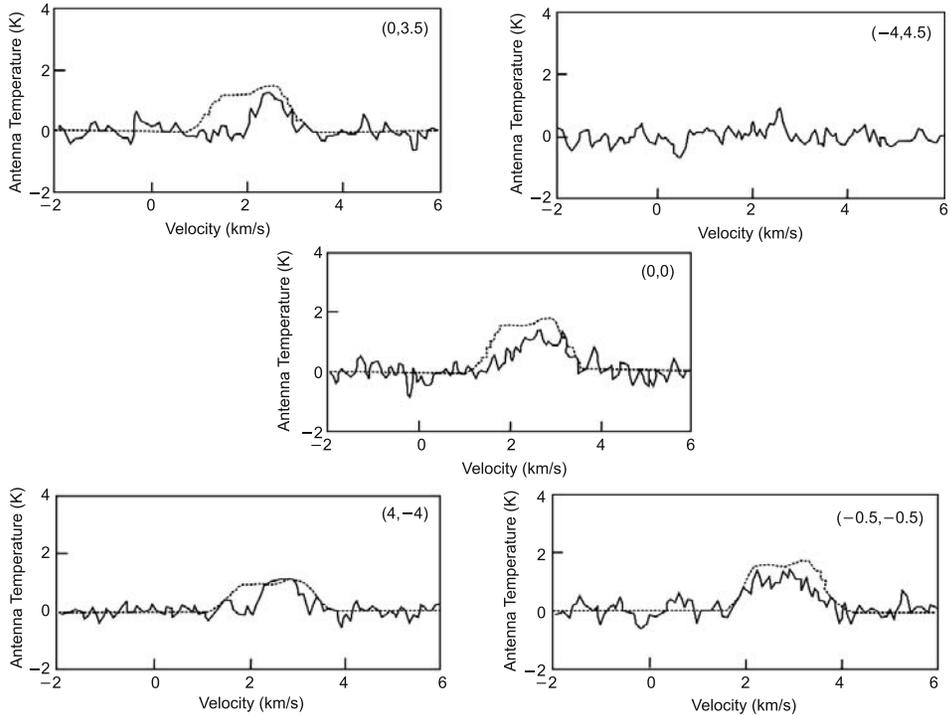
Figure 7. Comparison of modelled spectra (thick dotted line) with observed spectra (solid line) for $^{13}CO(3-2)$ line at few typical offset positions (mentioned within box) with respect to the $(0, 0)$ position (i.e., $15^h51^m30^s$, $-2^0 43'31''$). Scales are in X-axis velocity (km s^{-1}) and in Y-axis antenna temperature (K).

5. Conclusions

The main conclusions drawn from the comparison of observations with the 1D, RT models of the CO species are:

1. There exists a strong temperature gradient within the envelope of L183 with a kinetic temperature difference of ~ 7 K throughout the region, which suggests that the northern part of the cloud is cold relative to the southern part due to non-uniform illumination of the cloud by ISRF.
2. The signature of the spectra indicates the freeze-out of the molecules onto grains and thereby reducing the abundance at the very cold regions.
3. Possible contraction of core along the observed lines of sight.

References

Brown, P., Charnley, S., Millar, T. 1988, *MNRAS*, **231**, 409.

Caldwell, J. A. R. 1979, *A&A*, **71**, 255.

Dickens, J. E., Irvin, W. M., Snell, R. L., Bergin, E. A., Schloerb, F. P., Pratap, P., Miralles, M. P. 2000, *ApJ*, **542**, 870–889.

Guêlin, M., Langer, W. D., Wilson, R. W. 1982, *A&A*, **107**, 107.

Hogerheijde, M. R., van der Tak, F. F. S. 2000, *A&A*, **362**, 697–710.

Jian-Jun Zhou, Xing-Wu Zheng, Yu-Xi Chen 2001, *Chin. J. Astron. Astrophys.*, **1(3)**, 250–256.

Juvela, M., Mattila, K., Lehtinen, K., Lemke, D., Laureijs, R., Prusti, T. 2002, *A&A*, **382**, 583–599.

Laureijs, R. J., Clark, F. O., Prusti, T. 1991, *ApJ*, **372**, 185.

Miwa Goto, Tomonori Usuda, Naruhisa Takato, Masa Hayashi, Seiichi Sakamoto, Gaessler, W., Yutaka Hayano, Masanori Iye, Yukiko Kamata, Tomio Kanzawa, Naoto Kobayashi Yosuke Minowa, Ko Nedachi, Shin Oya, Pyo, T.-S., Saint-Jacques, D., Hiroshi Suto, Hideki Takami, Hiroshi Terada, George F. Mitchell 2003, *ApJ*, **598**, 1038–1047.

Marèchal, P., Pagani, L., Langer, W. D., Castets, A. 1997, *A&A*, **318**, 252–255.

Myers, P. C. 1980, *ApJ*, **242**, 1013.

Pagani, L., Langer, W. D., Castets, A. 1993, *A&A*, **274**, L13–L16.

Pagani, L., Pardo-Carrion, J. R., Stepnik, B. 2000, *Proc. Symposium "The Promise of the Herschel Observatory" Spain.*

Pagani, L., Lagache, G., Bacmann, A., Motte, F., Cambresy, L., Fich, M., Teyssier, D., Miville-Deschenes, M.-A., Pardo, J.-R., Apponi, J. A., Stepnik, B. 2003, *A&A*, **406**, L59–L62.

Pagani, L., Pardo, J.-R., Apponi, J. A., Bacmann, A., Cabrit, S. 2005, *A&A*, **429**, 181.

Pagani, L., Bacmann, A., Cabrit, S., Vastel, C. 2007, *A&A*, **467**, 179.

Roueff, E., Tine, S., Coudert, L. H., Pineu des Forets, G., Falgarone, E., Gerin, M. 2000, *A&A*, **354**, L63–L66.

Schöier, F. L., van der Tak, F. F. S., van Dishoeck, E. F., Black, J. H. 2005, *A&A*, **432**, 369–379.

Snell, R. L. 1981, *ApJS*, **45**, 121.

Snell, R. L., Langer, W. D., Frerking, M. A. 1982, *ApJ*, **255**, 149.

Swade, D. A. 1989a, *ApJS*, **71**, 219.

Swade, D. A. 1989b, *ApJ*, **345**, 828.

Vedi, K., Williams, I. P., White, G. J., Avery, L., Cronin, N. 1985, *LNP*, **237**, 83–86.

Willacy, K., Williams, D. 1993, *MNRAS*, **260**, 635.